INFRARED MICROSCOPY INVESTIGATION OF THE CRYSTAL STRUCTURE OF RIBBON GROWTH ON SUBSTRATE (RGS) SOLAR CELLS

U. Hess[1], S. Joos[1], S. Seren[1], G. Hahn[1], P.-Y. Pichon[2], A. Schönecker[2], T. Weber[3]

[1]University of Konstanz, Department of Physics, P.O. Box, 78467 Konstanz, Germany
[2]RGS Development B.V., P.O. Box 40, 1724 ZG Oudkarspel, The Netherlands
[3]SolarWorld Innovations GmbH, P.O. Box 1711, 09587 Freiberg, Germany

Author for correspondence: uwe.hess@uni-konstanz.de, Tel.: +49 7531 882132, Fax: +49 7531 883895

ABSTRACT: Ribbon Growth on Substrate (RGS) silicon is a multicrystalline ribbon material where the silicon wafers are casted directly out of the melt. The advantage referring to the standard block-casting of multicrystalline silicon is the avoidance of the time and energy intensive block-casting itself and the avoidance of material loss due to wafer wire sawing. Thus, the RGS process allows a cost effective silicon wafer production in combination with a very high production speed in the order of one wafer per second. The crystallization and casting characteristics limit the grain sizes of RGS wafers to values between 0.1 mm and 1 mm and the solar cell parameters are affected by a variety of crystal defects.
Due to its bandgap, silicon is transparent for infrared light with wavelengths > 1200 nm. However, crystal defects like grain boundaries, cracks and precipitates can scatter and absorb this light and therefore the shadowing can be investigated. The non-destructive method of Infrared Microscopy makes it possible to observe the actual spatial distribution and properties of certain defects in a three-dimensional way. The comparison of Infrared Microscopy, Electron Microscopy, EDX and etch pit density determination on the one hand and spatially resolved measurements like Light Beam Induced Current (LBIC) of the processed RGS solar cell on the other hand, were investigated. Defects found by Infrared Microscopy can be linked to oxygen and carbon impurities at grain boundaries but grain sizes and etch pit densities of grains have the strongest correlation to the local mean Internal Quantum Efficiency (IQE).
Keywords: Ribbon Silicon, Crystallization, Defect Density

1 INTRODUCTION

Ribbon Growth on Substrate (RGS) [1] wafers are up to now produced by a laboratory scale R&D installation in the Netherlands at ECN. Former investigations on crystal structure and electrical properties of RGS wafers and solar cells provided knowledge for a new industrial scale production machine. This new installation was built by RGS Development B.V. and is at the moment under integration and process testing. First RGS wafers from the new installation are delivered to R&D partners for testing and characterization. Figure 1 shows a photo of this test machine installation.

Figure 1: RGS industrial scale test machine installation at RGS Development B.V.

RGS wafers are grown directly on a substrate plate from the silicon melt [1]. Therefore it is a cost-effective method which avoids material losses due to wire sawing and time and energy consumption in relation to casting techniques like block-casting. However, the density of crystal defects like dislocations, grain boundaries and impurities which limit the as-grown minority charge carrier lifetimes [2,3] are higher compared to standard block-casted multicrystalline wafers.

Due to its bandgap, silicon is transparent for infrared light with energies below the bandgap (1,1 eV) but extended crystal defects like µ-cracks or grain boundaries can scatter and absorb the infrared light and appear as a shadowing of the image. An optical microscopy setup with an infrared camera was used to investigate shape, size and density of the observable crystal defects and Electron Microscopy, Energy Dispersive X-Ray analysis (EDX) and etch pit density determination was used to clarify the results. By moving the focal plane of the microscope it is possible to follow the three-dimensional structure of defects within the wafer. Figure 2 shows three Infrared Microscopy images of the same crystal defect but with different focal planes. The white circles and rectangles in the images emphasize optically focused parts of the defect structure. The right and the left image a & c are focused to the wafer front and back surfaces. The white circles mark particles on the surfaces which are used as reference points. The wafer is ~150 µm thick and the white rectangles in the middle of image (b) emphasize optically focused parts of the defect approximately 90 µm from the back surface within the wafer. Standard reflecting optical microscopy does not indicate a link of this defect to the wafer surfaces and is not observable with it.

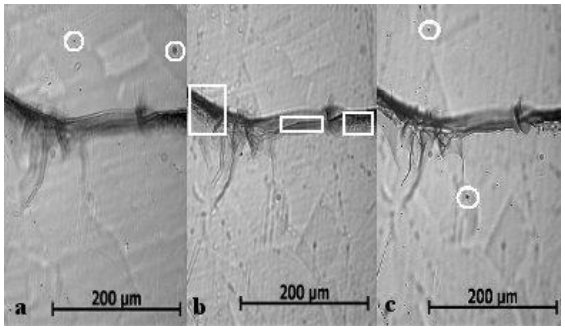

Figure 2: Three Infrared Microscopy pictures of the same crystal defect in a RGS wafer. The focal plane of the microscope setup was adjusted to (a) the front surface, (b) within the wafer and (c) the back surface. The white borders emphasize optical sharp parts.

2 CELL PROCESS AND CELL PROPERTIES

2.1 Cell Process

The RGS wafer investigated in this work was produced by a laboratory scale R&D machine at ECN. It is boron doped (3 Ωcm) and shows typical grain sizes in the order of 0.1 mm to 1 mm. Figure 3 shows the applied industrial type screen-printing solar cell process [4].

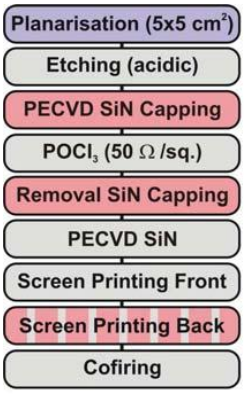

Figure 3: Process chart of the RGS solar cell (cell size: 5x5 cm^2) investigated in this work.

Even with the latest improvements in RGS wafer casting up to now it is beneficial for cell processing to planarize the as-grown wafers prior to processing to easily apply processing steps like screen-printing. Planarization means the mechanical leveling of the uneven wafer front side. It is sufficient to planarize the wafer until approximately 90% of the wafer surface is even. It is shown later that the remaining uneven (thinner) parts of the wafer surface do not have a direct influence on the local internal quantum efficiency (IQE). After planarization an acidic etching is applied to remove a defect-rich layer on the front and backside of the wafer. To avoid process induced shunting of the cells [4] an Al grid with 10% coverage is used for backside metallization in combination with a single side emitter, realized by a SiN capping layer on the backside before the phosphorous diffusion.

2.2 Cell Properties

Depending on the material quality, the shown cell process results in fill factors of ~75% and up to 13% efficiency [4]. The fill factors and therefore the efficiencies of RGS cells may be limited by low shunt resistances. Those shunt resistances can possibly be linked to crystal defects, which was another motivation for an Infrared Microscopy investigation of this material. The IV parameters of the RGS cell used in this work are shown in table I. A cell with a limited fill factor was chosen to ensure that microscopic defects can be found.

Table I: IV parameters of the RGS cells under investigation.

FF (%)	J_{sc} (mA/cm^2)	V_{oc} (mV)	η (%)
72	27.7	581	11.6

To gain knowledge of the local electrical properties of the cell a LBIC (figure 4) and an illuminated Lock-In Thermography [5,6] (figure 5) measurement was performed.

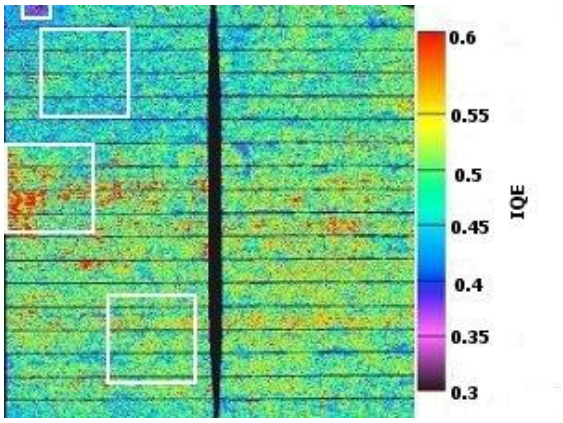

Figure 4: LBIC image of the RGS cell under investigation at a laser wavelength of 980 nm. The three white rectangles mark typical areas with a local mean IQE of 0.4 (top), 0.5 (bottom) and up to 0.6 in the middle square. The smaller white rectangle on the top emphasizes an area with a very low local IQE possibly because of metallization problems with an Al-grid finger of the open rear side metallization.

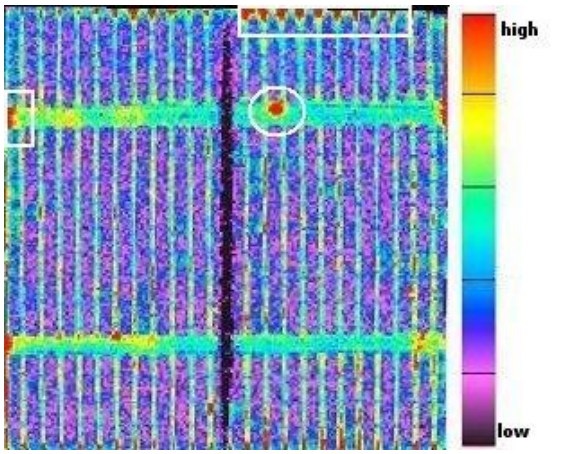

Figure 5: Illuminated Lock-In Thermography (iLIT) image of the same RGS cell. The Al backside grid

(horizontal bus bars) and the Ag front side bus bar (vertical, middle) are visible. The white borders indicate areas in which energy is dissipated by local defects.

LBIC image (figure 4) shows areas with different local mean IQE (white rectangles). A goal of the investigation was to determine differences in the crystallographic characteristics of those areas. The Lock-In Thermography image reveals hot spots (white borders) which are possibly linked to cell shunting. For the used cell process it is known that shunts are relatively often [7] linked to the metallization grids, respectively appear more often on areas where the Al grid on the back surface and the Ag grid on the front surface overlap. For the further statistical crystallographic investigations local mean IQE values in ~ 1x1 mm^2 areas were used to correlate the LBIC measurement with microscopic images.

3 CRYSTALLOGRAPHIC INVESTIGATIONS

3.1 Sample preparation

After processing and characterization of the cell, the metallization, ARC and emitter of the solar cell were etched for the investigation with Infrared and Electron Microscopy. Because of light scattering due to rough surfaces the wafer was polished on both surfaces. In the polishing step ~ 15-20 µm per side were removed and the remaining wafer had a thickness of ~150 µm. To determine the etch pit density, the polished wafer was treated with a Secco etch [8].

3.2 Infrared Microscopy

Figures 6-8 show Infrared Microscopy images. Figures 6a, b and 7 a, b are four exemplary images of typical areas of the wafer. Figure 6a shows grain structures and scratches on the surface. Figure 6b reveals distributed dark patterns which overlap with grain boundaries. Figure 7a shows lengthy patterns, which can be up to 1.5 mm long. Figure 7b shows an unplanarized part of the wafer.

Approximately 10% of the wafer area is not planarized and therefore not polished, which makes an investigation with Infrared Microscopy difficult. 60-70% of the wafer shows a similar structure like figure 6a. Patterns like figure 6b and 7a are distributed in areas equally all over the wafer. Generally these areas are up to 3-5 mm in diameter. The density (~ 10-20 objects/mm^2) and length (~ 50-300 µm) of objects in areas shown in figure 6b was measured. But neither the location of the area nor the density and average length could be correlated to the local mean IQE. The same applies to areas with lengthy patterns (up to ~1.5 µm long) shown in figure 7a. These lengthy patterns which can possibly be linked to carbon and oxygen impurities in grain boundaries as shown later using Electron Microscopy and EDX appear only in the pulling direction during wafer casting.

Figure 8a, b shows the remains of the back side Al grid of the open rear side metallization. Figure 8b indicates dent like structures (up to ~ 10 µm deep) on the wafer surface around dark patterns which overlap with the local grain boundaries (up to ~ 20-30 µm deep).

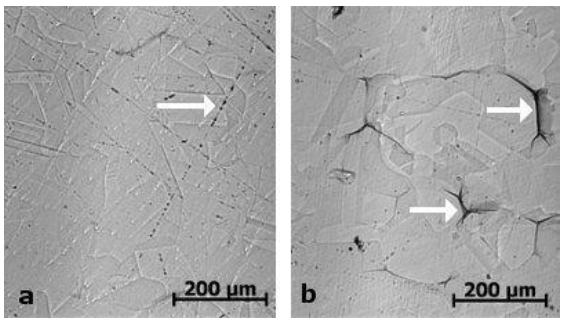

Figure 6: Infrared Microscopy images of two different areas of the wafer. The image on the left shows mainly the surface structure after polishing as well as grain boundaries. The white arrow points at a scratch, presumably originating from wafer polishing. White arrows in right part of the image point at scattered dark structures along grain boundaries.

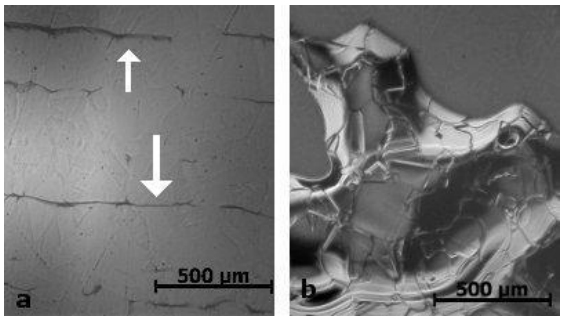

Figure 7: Infrared Microscopy images of two different areas of the wafer. White arrows in the left part point at lengthy parallel structures. The image on the right shows an unplanarized area of the wafer.

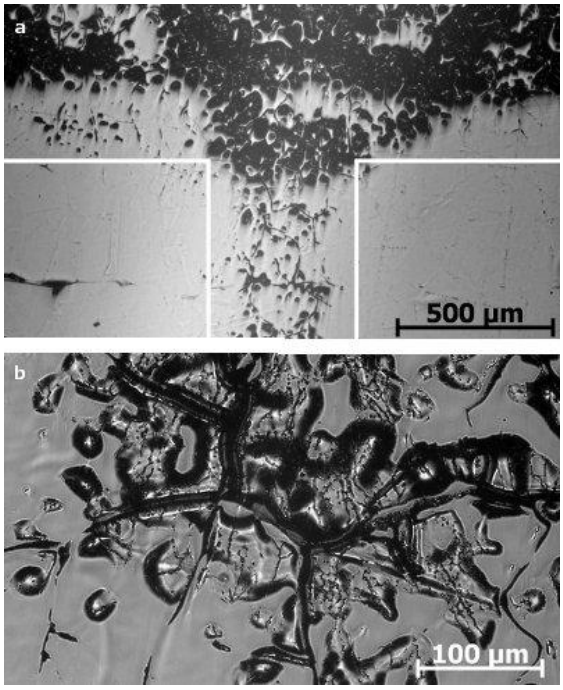

Figure 8: Infrared Microscopy image of the remains of a Al-grid bus bar and finger of the open rear side metallization after etching and polishing. The white

borders in the upper part emphasize the former bus bar (top, horizontal) and a grid finger (middle, vertical).The image at the bottom is a closer view on a part of the remains of the bus bar.

3.3 Electron Microscopy and EDX

Figure 9 and 10 are images of the wafer back surface with the remains of an Al grid bus bar. They indicate that grain boundaries are deepened in these regions. What seems like dust particles in the dent like structures distributed around the grain boundary in figure 9 can be found in any Al-grid area. Energy dispersive X-ray (EDX) analysis of these particles shows mostly silicon with an oxygen content of approximately 10% (mass percent). As indicated in figure 10, the grain boundaries in these areas can be deepened up to ~ 20-30 µm (from the polished wafer surface) by the local Al BSF formation.

Cross-sections of the wafer were prepared to investigate the crystal structure inside. Only a few disturbances of the otherwise flat polished intersections were observable. Figure 11 shows a pit (approximately 10 µm deep) along a grain boundary within the wafer. The location and distribution of these pits match the location and distribution of the lengthy patterns visible with Infrared Microscopy as shown in figure 7a. An EDX analysis reveals silicon with an oxygen content of approximately 5% and a carbon content of approximately 10% (mass percent). This strengthens the assumption that the dark patterns observed with Infrared Microscopy are impurities and inclusions originating from the casting process.

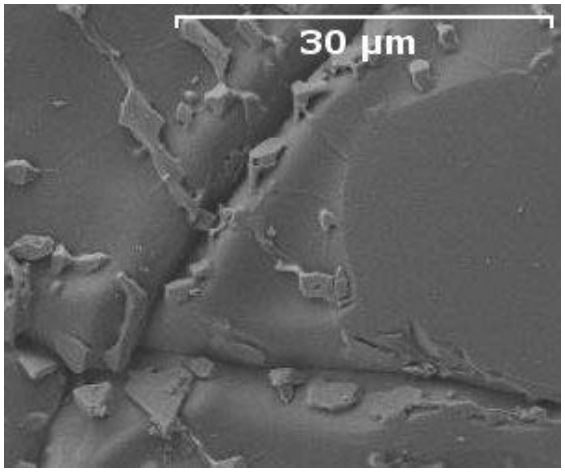

Figure 9: Electron Microscopy image of a deepened grain boundary in a wafer area with an Al bus bar on the backside of the wafer.

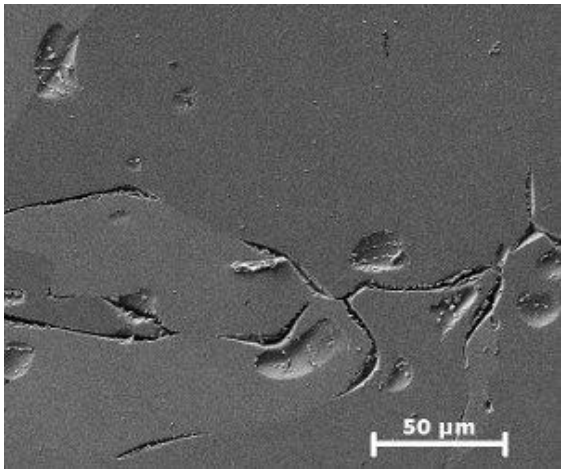

Figure 10: Electron Microscopy image of a grain boundary in a wafer area with an Al grid bus bar. The boundaries are deepened and surrounded by dent like structures.

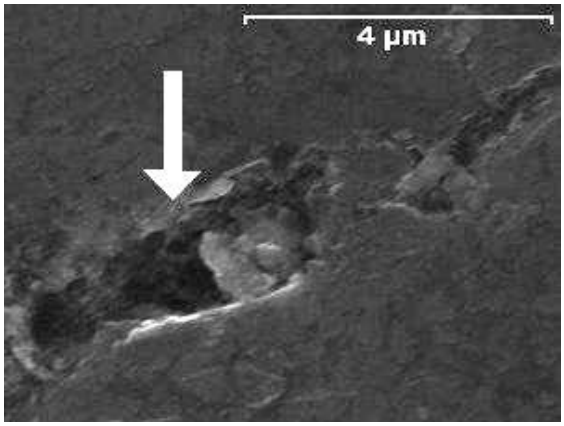

Figure 11: The white arrow in the Electron Microscopy image points a pit within the wafer.

3.3 Etch pit density

A Secco etch was applied to the polished wafers. This chemical treatment makes crystal defects like dislocations and grain boundaries observable. Figure12 is an image of a standard reflecting optical microscope setup. It shows the grain structure and different densities of crystal defects (small black spots) within the grains. Figure13 is an Infrared Microscopy image of a Secco etched wafer surface. With this technique it is possible to view the grain structure on front and back surface at the same time. Former investigations have shown a columnar growth of the grains [9] and a nearly equally distributed defect density within one grain. Figure13 shows that the grain boundaries are not exactly columnar but inclined. A correlation between the local mean IQE and areas with inclined grains could not be observed, but it is found that the dark patterns in figure6 and 7 are within grain boundaries.

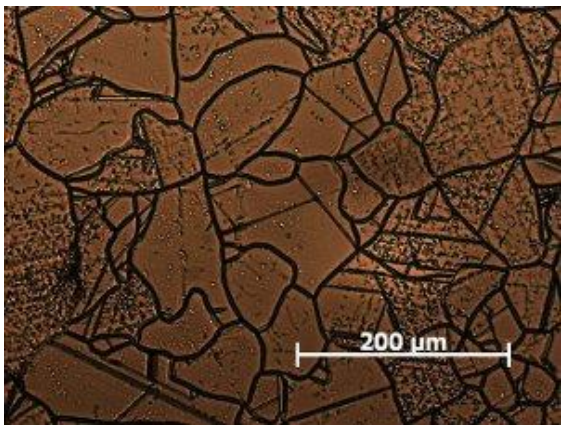

Figure 12: Optical Microscopy image of the polished wafer surface treated with Secco etch. It shows the grain structures and etch pits within the grains.

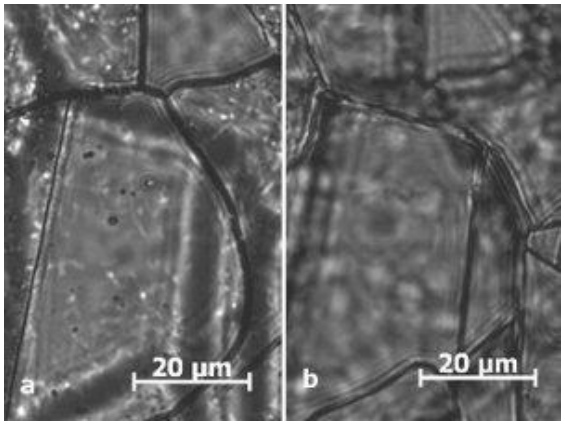

Figure 13: Infrared Microscopy image of the polished wafer surface treated with Secco etch. With this technique it is possible to view the grain structure on front and back surface at the same time. Looking from the front surface, on the left is the front side of the wafer and on the right the back side of the wafer.

4 DISCUSSION

The goal of this work was to correlate the different crystal characteristics to the local IQE. The size, distribution and density of the different dark patterns (figures 6 & 7) which were observable via Infrared Microscopy were investigated. But neither the location, the density, the shape nor the average length of these structures in a certain area could be correlated to a trend with the local IQE. But the patterns may be an upper limit to the local cell performance. The EDX analysis reveals carbon and oxygen impurities in pits shown in figure 11 which location and distribution fits to the lengthy patterns in figure 7a. But these can be found in areas with a limited local mean IQE of 0.4 as well as in areas with the highest mean IQE. The effect of those structures which are located in grain boundaries seems to be small or only very locally. Unplanarized and therefore thinner areas (up to ~ 100 µm) of the wafer are also distributed all over the wafer with no clear correlation to the local IQE.

Generally in wafer areas with an Al back surface grid, the chance to observe shunts with Lock-In Thermography is higher. The Infrared Microscopy image (figure 8) and the two Electron Microscopy images (figure 9 & 10) show a surface affected by dents and deepened grain boundaries within grid regions. These seem to be remains of the etched Al-Si BSF. The deepened grain boundaries which were observed up to 50-60 µm from the back surface to the wafer bulk (calculated from the unpolished processed cell) seem to fit the trend of an increased chance for shunts in this locations.

With the Secco etch technique the etch pit density, the grain size and grain proportion were investigated. Table II shows the mean local IQE and the corresponding average grain size.

Table II: Statistical comparison of the mean local IQE with local grain sizes in areas with white rectangles in figure 4.

Local IQE	0.6	0.5	0.4
Grain size	0.1 mm^2	0.07 mm^2	0.03 mm^2

Figure 12 is an exemplary picture which shows that the magnitude of the etch pit density is generally constant in one grain. The grains with less etch pits like in the middle of figure 12 have a density up to 10^4 $pits/cm^2$ (called low density grains). Grains on the right and on the left side in figure 12 have an etch pit density of above 10^6 $pits/cm^2$ (called high density grains). Table III shows the comparison of the local mean IQE in an area to the corresponding proportion low density gains to high density grains.

Table III: Comparison of the local mean IQE to the proportion of low density grains (etch pit density up to 10^4 $pits/cm^2$) to high density grains (etch pit density above 10^6 $pits/cm^2$).

Local IQE	0.6	0.5	0.4
Low / High	5-10	0.5	0.1-0.05

The local average IQE seems to be clearly linked to the grain sizes and the proportion of number of grains with less defects.

The distribution of dark patterns in grain boundaries observed with Infrared Microscopy, the oxygen and carbon impurities found with EDX, the unplanarized thinner areas of the wafer may limit the local IQE to a certain level, but the only clear correlation of the local mean IQE and crystallographic characteristic are in this case the local etch pit density and the grain size.

5 SUMMARY

The Ribbon Growth on Substrate method is a cost-effective casting technology with advantages in time, energy and material consumption compared to the standard block-casting process for multicrystalline silicon materials. Due to the crystallization characteristics a variety of crystal defects are observable in the wafer. The electrical properties of a processed RGS solar cell by means of LBIC measurement was compared to the Infrared Microscopy, Electron Microscopy, EDX and

Etch pit density investigations of the corresponding wafer. The structures and impurities found with these methods may limit the performance of the cell, but only etch pit density and the average grain size in a specific area of the wafer could be directly correlated to the local mean IQE. It could be found that the larger the grains and the lower the etch pit density in a certain area, the higher the local mean IQE.

6 OUTLOOK

The methods used to determine the crystallographic characteristics can be refined with high resolution EBIC / LBIC measurements to gain a deeper knowledge about the correlations between crystallographic characteristics and electrical properties. But the main investigation in the future will be the monitoring of different crystallization parameters of the casting of RGS wafers with the crystallographic parameters and their correlation to the local IQE and the passivation of defects by gettering und hydrogenation.

7 ACKNOWLEDGEMENTS

Part of this work was funded by the BMU in the OP-RGS (0325056) and the project (0325079). RGS test wafer manufacturing and crystal growth development are supported by SenterNovem within the EOS:ES program (IS073012). The content of this publication is the responsibility of the authors.

8 REFERENCES

[1] H. Lange, I.A. Schwirtlich, Ribbon Growth on Substrate (RGS) - A new approach to high speed growth of silicon ribbons for photovoltaics, J. Cryst. Growth 104 (1990)
[2] G. Hahn, A. Schönecker, New crystalline silicon ribbon materials for photovoltaics, J. Phys.: Condens. Matter 16 (2004)
[3] S. Seren, M. Kaes, G. Hahn, A. Gutjahr, A.R. Burgers, A. Schönecker, Efficiency potential of RGS silicon from current R&D production, Proc. 22nd EC PVSEC, 854, (2007) Milan
[4] S. Seren et al., Ribbon Growth on Substrate – A roadmap to higher efficiencies, Proc. 21th EC PVSEC, 668, (2006) Dresden
[5] O. Breitenstein, M. Langenkamp, Lock-In Thermography: Basics and Use for Functional Diagnostics of Electronic Components, Springer 2003
[6] M. Käs, S. Seren, T. Pernau, G. Hahn, Light-modulated Lock-In Thermography for photosensitive pn-Structures and Solar Cells, Prog. Photovolt.: Res. Appl. 12(5), 355, (2004)
[7] S. Seren, G. Hahn, A. Gutjahr, A. R. Burgers, A. Schönecker, Screen-printed ribbon growth on substrate solar cells approaching 12% efficiency, Proc. 20th EC PVSEC, 1055- 1058, (2005), Barcelona
[8] D. G. Schimmel, A Comparison of Chemical Etches for Revealing <100> Silicon Crystal Defects, J. Electrochem. Soc., 123, Issue 5, pp. 734-741, (1976)
[9] U. Hess, T. Lauermann, S. Seren, G. Hahn, A. Schönecker Impact of the Crystal Structure on Solar Cell Parameters of Ribbon Growth on Substrate (RGS) Solar Cells, Proc. 23rd EC PVSEC, (2008), Valencia